

# Phi Meson Production in Heavy-Ion Collisions at SIS Energies

W. S. Chung<sup>1</sup>, G. Q. Li<sup>1,2</sup>, and C. M. Ko<sup>1</sup>

<sup>1</sup>*Department of Physics and Cyclotron Institute, Texas A&M University,  
College Station, Texas 77843, U.S.A.*

<sup>2</sup>*Department of Physics, State University of New York at Stony Brook,  
Stony Brook, New York 11794, U.S.A.*

## Abstract

Phi meson production in heavy-ion collisions at SIS/GSI energies ( $\sim 2$  GeV/nucleon) is studied in the relativistic transport model. We include contributions from baryon-baryon, pion-baryon, and kaon-antikaon collisions. The cross sections for the first two processes are obtained in an one-boson-exchange model, while that for the last process is taken to be of Breit-Wigner form through the phi meson resonance. The dominant contribution to phi meson production in heavy ion collisions at these energies is found to come from secondary pion-nucleon collisions. Effects due to medium modifications of kaon masses are also studied and are found to reduce the phi meson yield by about a factor of two, mainly because of increased phi decay width as a result of dropping kaon-antikaon masses. In this case, the  $\phi/K^-$  ratio is about 4%, which is a factor of 2-3 below preliminary experimental data from the FOPI collaboration at GSI. Including also the reduction of phi meson mass in medium increases this ratio to about 8%, which is then in reasonable agreement with the data.

## I. INTRODUCTION

There are increasing interests in phi meson production from heavy ion collisions since the suggestion by Shor [1] that an enhanced production may signal the formation of a quark-gluon plasma in these collisions as its production in hadronic matter is usually suppressed by the OZI rule [2]. However, recent theoretical studies have suggested that because of chiral symmetry restoration hadron properties are expected to change in hot dense hadronic matter [3–5] (For recent reviews see Refs. [6–8]). For phi meson in dense matter, QCD sum rule calculations have shown that its mass decreases by about 2-3% at normal nuclear matter density [4]. Reduced in-medium phi meson mass has also been predicted in vector dominance model with dropping kaon masses [9], in hadronic models that include the particle-antiparticle vacuum polarization [10], and in hidden gauge theory [11]. A reduced phi meson mass in medium is expected to enhance its yield from heavy ion collisions even in the absence of the quark-gluon plasma [12]. In this case, one can also study the phi meson in-medium properties via the dilepton spectrum from these collisions as pointed out in Refs. [4,13,14]. At high temperature, the reduction of phi meson mass may become more appreciable because of the decrease of strangeness condensate  $\langle \bar{s}s \rangle$  as a result of the presence of strange hadrons [5]. It has thus been suggested that a low mass phi peak besides the normal one may appear in the dilepton spectrum from ultrarelativistic heavy ion collisions if a first-order phase transition or a slow cross-over between the quark-gluon plasma and the hadronic matter occurs in the collisions [15].

Experimentally, phi meson production has been studied at SPS/CERN by the NA38 collaboration [16] and the HELIOS-3 collaboration [17] using a proton or sulfur projectile at 200 AGeV and a tungsten or uranium target. A factor of 2 to 3 enhancement in the double ratio  $(\phi/(\omega + \rho^0))_{SU(W)}/(\phi/(\omega + \rho^0))_{pW}$  has been observed. Various theoretical attempts have been made to understand this enhancement [12,18,19]. In particular, an enhancement of phi meson yield may be a signature of the formation of a quark gluon plasma in the collisions [1]. However, the enhancement can also be explained in hadronic models if one

takes into account the reduced phi meson mass in medium [12]. In Ref. [18], the color rope fragmentation and hadronic rescattering have been introduced to understand the observed phi meson enhancement.

Phi mesons have also been measured at AGS/BNL by the E-802 collaboration in central collisions between a 14.6 AGeV/c Si beam and a Au target [20]. They are identified from the invariant mass spectrum of  $K^+K^-$  pairs, and the measured phi meson mass and width are consistent with that in free space. The ratio of the phi meson yield to the  $K^-$  yield has been found to be about 10%, which can be understood if thermal and chemical equilibrium are assumed at freeze out with a temperature of about 110 MeV [21,22]. On the other hand, calculations by Baltz and Dover [23] based on the coalescence model, in which the phi meson is formed from the kaon and antikaon at freeze out, underestimate the data by a large factor.

Phi mesons from heavy-ion collisions at SIS/GSI energies are being studied by the FOPI collaboration [24] also through the  $K^+K^-$  invariant mass distribution. About 30 phi mesons have been identified in central collisions of Ni+Ni at 1.93 AGeV. Based on these preliminary results it has been concluded that the phi meson yield is about 10% of the  $K^-$  yield, which is very similar to that observed at the AGS energies. This is somewhat surprising since the SIS energies are below the phi meson production threshold in the nucleon-nucleon collision in free space, while the AGS energies are well above the threshold.

In this paper, we shall carry out a detailed transport model study on phi meson production in heavy-ion collisions at SIS energies. There are mainly two reasons to work at these energies. First, particle production at subthreshold energies is sensitive to medium modifications of hadron properties [7,8,25,26]. Secondly, the reaction dynamics of heavy-ion collisions at SIS energies is relatively simple compared to that at higher energies as it involves mainly the nucleon, delta, and pion. In a previous study of phi meson production at SIS energies [14], only the contribution from the reaction  $K\bar{K} \rightarrow \phi$  has been included, and the  $\phi/K^-$  ratio is predicted to be less than 1%, which is an order of magnitude smaller than the experimental result from the FOPI collaboration. To explain this large discrepancy we include here phi meson production also from baryon-baryon and pion-baryon collisions.

The cross sections for these processes are calculated using an one-boson-exchange model with parameters fitted to available experimental data. Some results from this study have been reported earlier [27]. We find that in heavy ion collisions the dominant contribution to phi meson production is from the  $\pi N$  collision, and its inclusion in the transport mode brings the predicted  $\phi/K^-$  ratio closer to the measured one by the FOPI collaboration. Furthermore, we study the effect of medium modifications of kaon properties on phi meson production. Kaplan and Nelson have pointed out that the kaon mass changes in nuclear matter [28]. In chiral perturbation theory, the kaon mass is predicted to increase slightly while the antikaon mass decreases significantly as the density increases [29]. Overall, the total mass of a kaon-antikaon pair is lowered in dense matter. This affects appreciably the phi decay width  $\Gamma_{\phi \rightarrow K\bar{K}}$ , which is only about 3.7 MeV in free space, since the phi meson mass is very close to twice the kaon mass. A reduced kaon in-medium mass thus increases  $\Gamma_{\phi \rightarrow K\bar{K}}$ , so phi mesons are more likely to decay before freeze out, leading to a lower final phi meson yield. This reduction is, however, compensated by effects from the dropping phi meson in-medium mass.

The paper is organized as follows: In section II we calculate the elementary cross sections for phi meson production and absorption using an one-boson-exchange model. Section III describes the nucleon, pion and kaon dynamics in heavy ion collisions using the relativistic transport model. Results on the phi meson yield and distributions from these collisions are given in section IV. Section V is the summary and outlook.

## II. ELEMENTARY CROSS SECTIONS

For heavy ion collisions at SIS energies, the most abundant particles are the nucleon,  $\Delta$  resonance, and pion. Phi meson can thus be produced from reactions such as  $NN \rightarrow NN\phi$ ,  $N\Delta \rightarrow NN\phi$ ,  $\Delta\Delta \rightarrow NN\phi$ ,  $\pi N \rightarrow \phi N$ , and  $\pi\Delta \rightarrow \phi N$ . The production of phi meson from  $\pi\pi$  scattering is expected to be unimportant due to its higher production threshold than that for the other reactions, and is thus ignored. Although both kaon and antikaon are only

scarcely produced, phi meson production from the reaction  $K\bar{K} \rightarrow \phi$  turns out nonnegligible in the case of using in-medium kaon masses and will be included.

Unfortunately, the cross sections for these reactions are not well-known empirically. There exist some data for the  $\pi N$  channel near threshold [30], but the  $NN$  channel has been studied only at high energies [31]. Because of the scarcity of experimental data, an one-boson exchange model has been introduced in Ref. [27] to extrapolate from the data at high energies to make predictions at energies near the production threshold, and also to calculate the cross sections for reactions involving the delta resonance as they cannot be measured experimentally. In that study, only the lowest order Born amplitude for phi meson production are considered, and this should be a reasonable approximation to the full amplitude because phi meson production has a very small probability in these reactions. In the following, we discuss this model and its predictions for both phi production and absorption cross sections.

The interaction Lagrangians needed in the one-boson exchange model are well-known, and they are given by

$$\mathcal{L}_{\pi NN} = -\frac{f_{\pi NN}}{m_\pi} \bar{\psi} \gamma^5 \gamma^\mu \vec{\tau} \psi \cdot \partial_\mu \vec{\pi}, \quad (1)$$

$$\mathcal{L}_{\rho NN} = -g_{\rho NN} \bar{\psi} \gamma^\mu \vec{\tau} \psi \cdot \vec{\rho}_\mu - \frac{f_{\rho NN}}{4m_N} \bar{\psi} \sigma^{\mu\nu} \vec{\tau} \psi \cdot (\partial_\mu \vec{\rho}_\nu - \partial_\nu \vec{\rho}_\mu), \quad (2)$$

$$\mathcal{L}_{\rho N\Delta} = i \frac{f_{\rho N\Delta}}{m_\rho} \bar{\psi} \gamma^5 \gamma^\mu \vec{T} \psi^\nu \cdot (\partial_\mu \vec{\rho}_\nu - \partial_\nu \vec{\rho}_\mu) + \text{h.c.}, \quad (3)$$

$$\mathcal{L}_{\pi\rho\phi} = \frac{f_{\pi\rho\phi}}{m_\phi} \epsilon_{\mu\nu\alpha\beta} \partial^\mu \vec{\phi}^\nu \partial^\alpha \rho^\beta \cdot \vec{\pi}. \quad (4)$$

In the above,  $\psi$  is the nucleon field with mass  $m_N$ ;  $\psi_\mu$  is the Rarita-Schwinger field for the spin-3/2 delta resonance with mass  $m_\Delta$ ; and  $\pi$ ,  $\rho_\mu$ ,  $\phi_\mu$  are meson fields with masses  $m_\pi$ ,  $m_\rho$ ,  $m_\phi$ , respectively. The isospin matrices, Dirac  $\gamma$ -matrices, and Levi-Civita tensor are denoted by  $\vec{\tau}$ ,  $\gamma^\mu$ , and  $\epsilon^{\mu\nu\alpha\beta}$ , respectively. The coupling constants and cutoff parameters in  $\mathcal{L}_{\pi NN}$ ,  $\mathcal{L}_{\rho NN}$ , and  $\mathcal{L}_{\rho N\Delta}$  are taken from the Model II of Table B.1 in Ref. [32]. From the measured width  $\Gamma_{\phi \rightarrow \pi\rho} \approx 0.6$  MeV, the coupling constant  $f_{\pi\rho\phi} \approx 1.04$  is determined.

### A. Phi meson production from pion-baryon collisions

The Feynman diagrams for the reactions  $\pi N \rightarrow \phi N$  and  $\pi \Delta \rightarrow \phi N$  are shown in Fig. 1. A monopole form factor is introduced at the  $\pi \rho \phi$  vertex, i.e.,

$$F(q_\pi, q_\rho) = \frac{(\Lambda_{\pi \rho \phi}^\pi)^2 - m_\pi^2}{(\Lambda_{\pi \rho \phi}^\pi)^2 + q_\pi^2}. \quad (5)$$

The cut-off parameter  $\Lambda_{\pi \rho \phi}^\rho$  is adjusted to give a reasonable fit to the experimental data from the reaction  $\pi^- p \rightarrow n \phi$  [30], and a value of 1.2 GeV is obtained. The comparison between calculated results and the experimental data as well as the parameterization by Sibirtsev [33] can be found in Ref. [27].

Since the isospin degree of freedom is usually not explicitly treated in transport model, we have thus calculated the isospin-averaged cross sections for  $\pi N \rightarrow \phi N$  and  $\pi \Delta \rightarrow \phi N$ . The results are shown in Fig. 2. Near threshold the cross section for  $\pi N \rightarrow \phi N$  is seen to be much larger than the cross section for  $\pi \Delta \rightarrow \phi N$  as a result of the strong tensor coupling at the  $\pi NN$  vertex.

To determine the momentum of produced phi meson in the transport model, we also need the differential cross sections for these reactions. Since only two particles are in the final state, the magnitude of the phi momentum is fixed by kinematics. The differential cross section  $d\sigma/d\cos\theta$  for these reactions at an energy of 0.2 GeV above the threshold is shown in Fig. 3.

### B. phi meson production from baryon-baryon collisions

The Feynman diagrams for the reactions  $NN \rightarrow NN\phi$ ,  $N\Delta \rightarrow NN\phi$ , and  $\Delta\Delta \rightarrow NN\phi$  are shown in Fig. 4. Exchange diagrams are also included as the two final nucleons are identical. There is some ambiguity in treating the  $\pi \rho \phi$  vertex in Fig. 4, which involves two virtual particles. Such a vertex does not exist in the Bonn potential model, and there is also no theoretically well-defined criteria for prescribing its form. The following form has been used in Ref. [27],

$$F(q_\pi, q_\rho) = \left( \frac{(\Lambda_{\pi\rho\phi}^\pi)^2 - m_\pi^2}{(\Lambda_{\pi\rho\phi}^\pi)^2 + q_\pi^2} \right) \left( \frac{(\Lambda_{\pi\rho\phi}^\rho)^2 - m_\rho^2}{(\Lambda_{\pi\rho\phi}^\rho)^2 + q_\rho^2} \right), \quad (6)$$

where  $q_\rho$  and  $q_\pi$  are four momenta of the virtual  $\rho$  and  $\pi$  meson, respectively. The cut-off parameter  $\Lambda_{\pi\rho\phi}^\rho$  is the same one introduced earlier in calculating the cross section for  $\pi N \rightarrow \phi N$ . The other cut-off parameter  $\Lambda_{\pi\rho\phi}^\pi$  is introduced to take into account the virtuality of the pion. The cross section for  $pp \rightarrow pp\phi$  has been measured at several energies [31], and the one at the lowest energy has been used in Ref. [27] to fix  $\Lambda_{\pi\rho\phi}^\pi$ , and a value of 0.95 GeV has been obtained. Comparisons of calculated results with both experimental data and the results by Sibirtsev based on an one-pion exchange model [33] have been given in Ref. [27]. We note that both  $\Lambda_{\pi\rho\phi}^\rho$  and  $\Lambda_{\pi\rho\phi}^\pi$  are in the order of 1 GeV, similar to typical values for cut-off parameters in both the Bonn potential model and other hadronic models.

For the reactions  $N\Delta \rightarrow NN\phi$  and  $\Delta\Delta \rightarrow NN\phi$ , the exchanged pion can be on shell, so the cross sections are singular in certain kinematical region. This singularity can be regulated by the Peierls method [34], in which the energy of the delta resonance is taken to be complex to account for its finite lifetime. As a result, the four-momentum of the exchanged pion acquires an imaginary part, which thus renders the pion propagator finite at the pion pole.

The isospin averaged cross sections for phi meson production from baryon-baryon collisions are shown in Fig. 5. There are significant differences between the cross sections for the reactions  $NN \rightarrow NN\phi$ ,  $N\Delta \rightarrow NN\phi$ , and  $\Delta\Delta \rightarrow NN\phi$ . Near threshold, all are much smaller than the cross section for phi meson production from pion-nucleon collisions.

Since there are three particles in the final state in baryon-baryon collisions, the momentum of produced phi meson is given by the triple differential cross sections  $d^3\sigma/dp_x dp_y dp_z$  or double differential cross section  $d^2\sigma/p^2 dp d\Omega$  if there is an azimuthal symmetry. To simplify the numerical procedure, we introduce the assumption that the phi meson momentum is isotropic in baryon-baryon center-of-mass frame. We then need only the momentum spectrum  $d\sigma/dp$ , which is shown in Fig. 6 for these reactions again at an energy of 0.2 GeV above the threshold.

### C. Phi meson production from kaon-antikaon annihilation

The total cross section for  $K\bar{K} \rightarrow \phi$  is assumed to have a Breit-Wigner form as in Ref. [14], i.e.,

$$\sigma(K\bar{K} \rightarrow \phi) = \frac{3\pi}{k^2} \frac{(m_\phi \Gamma_\phi)^2}{(M^2 - m_\phi^2)^2 + (m_\phi \Gamma_\phi)^2}, \quad (7)$$

where  $\Gamma_\phi$  is the phi meson decay width to  $K\bar{K}$  and is given by

$$\Gamma_\phi = \frac{g_{\phi K\bar{K}}^2}{4\pi} \frac{(m_\phi^2 - 4m_K^2)^{3/2}}{6m_\phi^2}, \quad (8)$$

with the coupling constant  $g_{\phi K\bar{K}}^2/4\pi \approx 1.69$  determined from the empirical width of 3.7 MeV. In using Eq. (7), we have thus neglected the small effect due to the decay of phi meson into other channels.

### D. Phi meson scattering by nucleons

Once a phi meson is produced, there are three kinds of reactions it can take part in: decay, inelastic and elastic scattering by nucleons. The dominant decay mode of phi meson is  $\phi \rightarrow K\bar{K}$ , with a decay width given by Eq. (8). Here we only consider phi meson absorption due to  $\phi N$  collisions as that due to  $\phi\pi$  and  $\phi\Delta$  scattering is expected to be insignificant because of the low pion and delta densities compared with that of nucleons (see Fig. 8). We have included the reactions  $\phi N \rightarrow K\Lambda$ ,  $\phi N \rightarrow \rho N$ ,  $\phi N \rightarrow \pi N$ , and  $\phi N \rightarrow \pi\Delta$ . The cross section for the first reaction is related via detailed balance to that of  $\Lambda K \rightarrow \phi N$ , which has already been calculated in Ref. [12] based on a kaon exchange model with parameters taken from Ref. [35]. The reaction  $\phi N \rightarrow K\Sigma$  is neglected since the  $N\Sigma K$  coupling constant ( $g_{N\Sigma K}^2/4\pi \sim 0.6$ ) is much smaller than that of  $N\Lambda K$  ( $g_{N\Lambda K}^2/4\pi \sim 16$ ) [35]. The cross section for the other three reactions can be obtained from those for  $\rho N \rightarrow \phi N$ ,  $\pi N \rightarrow \phi N$ , and  $\pi\Delta \rightarrow \phi N$  using detailed balance relations. We have already determined in the above the cross sections for phi meson production from pion-baryon collisions. For the reaction  $\rho N \rightarrow \phi N$ , we simply interchange the pion and rho meson in the first diagram of Fig. 1.



The cross sections for these phi meson absorption processes are summarized in Fig. 7. We see that  $\phi N \rightarrow K\Lambda$  is the dominant one as already pointed out in Refs. [1,12], because this is the only one among the four reactions that is not suppressed by the OZI rule .

The phi-nucleon elastic scattering is also included. Experimentally, the cross section for this process can be extracted from data on phi meson photoproduction using the vector meson dominance model [36]. In the energy range  $3.5 \text{ GeV} < p_{\text{lab}} < 5.8 \text{ GeV}$ , a value of 0.56 mb has been obtained. Here we make the rough approximation that the cross section is a constant of 0.56 mb in the energy range considered. We note that a slightly larger value has been obtained in Ref. [37]. The phi-nucleon scattering does not change the phi meson yield, but affects its momentum distribution. Since this cross section is rather small, the effect is not appreciable as shown below.

### E. Discussions

So far we have calculated exclusive phi meson production cross sections with no pions in the final state. In principle, phi meson can also be produced in association with one or more pions, and one needs for heavy-ion collisions inclusive cross sections such as  $NN \rightarrow \phi X$ . Since the beam energies we consider in this work are below the phi meson production threshold in nucleon-nucleon collision, we expect that exclusive reactions such as  $NN \rightarrow NN\phi$ , which have lower thresholds, are more important than the ones with pions in the final state, which require additional energies and are thus suppressed.

We would like to point out that in spite of the success of the one-boson-exchange model at low energies, this model has not been carefully verified at energies above the phi meson production threshold. It is often believed that the quark degree of freedom becomes relevant at a kinetic energy of 1-2 GeV, so it is not known if our procedure of using the data point at  $p_{\text{lab}} = 10 \text{ GeV}$  to fix the cross section for  $pp \rightarrow pp\phi$  near the threshold is reliable. Nevertheless, this model has been used quite often in calculating the cross sections for pion production [38], eta production [39], kaon production [40,41], and baryon resonance

excitations [42] from nucleon-nucleon collisions in this energy region. Measurements of  $pp \rightarrow pp\phi$  at low energies are being carried out at SATURNE [43], and these data will be very useful in testing the validity of our model. With this caveat in mind, we proceed to our transport model study using the above elementary cross sections.

### III. THE NUCLEON, PION AND KAON DYNAMICS

#### A. The relativistic transport model

For the description of heavy-ion collisions at SIS energies, we use the relativistic transport model (RVUU) developed in Ref. [44] from the non-linear  $\sigma - \omega$  model [45] and extensively used in previous studies. At these energies, the colliding system consists mainly of nucleons, delta resonances, and pions. While medium effects on pions are neglected as in most transport models, nucleons and delta resonances propagate in a common mean-field potential according to Hamilton equations of motion, i.e.,

$$\frac{d\mathbf{x}}{dt} = \frac{\mathbf{p}^*}{E^*} \quad \frac{d\mathbf{p}}{dt} = -\nabla_{\mathbf{x}}(E^* + (g_{\omega}/m_{\omega})^2 \rho_B), \quad (9)$$

where  $E^* = (m^{*2} + \mathbf{p}^{*2})^{1/2}$ . The effective mass and kinetic momentum of a baryon are given, respectively, by  $m^* = m - g_{\sigma}\langle\sigma\rangle$  and  $\mathbf{p}^* = \mathbf{p} - g_{\omega}\langle\boldsymbol{\omega}\rangle$ , where the expectation values  $\langle\sigma\rangle$  and  $\langle\boldsymbol{\omega}\rangle$  are related to the attractive scalar potential and the vector current of a baryon in nuclear matter. We use in this work the parameter set that corresponds to the soft equation of state [46] with a compressibility  $K = 200$  MeV and an effective nucleon mass  $m_N^* = 0.83 m_N$  at normal nuclear density. These particles also undergo stochastic two-body collisions, including both elastic ( $NN \rightarrow NN$ ,  $N\Delta \rightarrow N\Delta$ ,  $\Delta\Delta \rightarrow \Delta\Delta$ ) and inelastic ( $NN \leftrightarrow N\Delta$ ,  $\Delta \leftrightarrow N\pi$ ) scattering. The standard Cugnon parameterization [47] and proper detailed-balance prescription [48] are used for describing these reactions.

Besides pions, other particles are also produced in heavy-ion collisions. However, their production probabilities are very small at these energies, and they can thus be treated perturbatively, in the sense that their production and interactions do not affect the dynamics

of nucleons, delta resonances, and pions. This is carried out using the perturbative test particle method of Ref. [49,50]. In the case of kaons, they are produced from pion-baryon and baryon-baryon collisions whenever the energy is above the threshold. Then, a probability factor given by the kaon production cross section to the total pion-baryon or baryon-baryon cross section is assigned to the produced kaon. The motion and collision of the kaon are then followed. However, only the kaon momentum is changed after a kaon-nucleon collision. This method allows us to include easily the medium effects on the kaon as shown in Ref. [49]. We use in this study the kaon in-medium mass obtained from the mean-field approximation to chiral Lagrangian [28]. As in Ref. [51], the kaon mass  $m_K^*$  at nuclear matter density  $\rho$  is given by

$$m_K^* = m_K \left[ 1 - \frac{\Sigma_{KN}}{f^2 m_K^2} \rho_s + \left( \frac{3}{8} \frac{\rho}{f^2} \right)^2 \frac{1}{m_K^2} \right]^{1/2} + \frac{3}{8} \frac{\rho}{f^2}. \quad (10)$$

In the above,  $m_K$  is the kaon mass in free space;  $f \approx 93$  MeV is the pion decay constant; and  $\rho_s$  is the nuclear scalar density. The kaon-nucleon sigma term is denoted by  $\Sigma_{KN}$  and is taken to be about 350 MeV. At normal nuclear density, the kaon mass is then increased by about 10 MeV. For antikaon, its vector interaction is opposite to that of kaon, so the last term in Eq. (10) has instead a negative sign. The antikaon mass at normal nuclear density is reduced by about 100 MeV. Corrections to the mean-field results may not be negligible [29,52] and are still under debate. Since there are other uncertainties in the treatment of kaons such as their production cross sections from baryon-baryon collisions, we will not address the sensitivity of our results on these corrections.

Our treatment of kaon follows essentially Refs. [50,51,53], where the baryon-baryon production channels  $BB \rightarrow N\Lambda K$  and  $BB \rightarrow N\Sigma K$  are included with their cross sections given by the Randrup and Ko parameterization [54]. We have also included the pion-baryon channels  $\pi N \rightarrow \Lambda K$  and  $\pi N \rightarrow \Sigma K$ . For these cross sections, the parameterizations due to Cugnon [55] are used. Kaon production from  $\pi\Delta$  collisions is neglected as its cross section has been shown to be much smaller than that for  $\pi N$  collisions [56].

The production of antikaon in heavy-ion collisions at SIS energies was first studied in Ref.

[57] using the relativistic transport model and the Zwermann-Schürmann [58] parameterization for the antikaon production cross section from the nucleon-nucleon collision. However, it has been recently found that this parameterization overestimates the cross sections near the threshold by about one order of magnitude [59,60], and contributions from pion-hyperon interactions [61], which were neglected in Ref. [57], are needed to account for the measured  $K^-$  yield. In this work, we have thus modified our earlier treatment of antikaon production by using instead the parameterizations proposed in Ref. [59] for antikaon production cross sections in both pion-baryon and baryon-baryon collisions. We have also included contributions from the pion-hyperon collisions.

### B. The pion and nucleon yield and distributions

In the upper window of Fig. 8, we show the time evolution of central baryon and pion densities in Ni+Ni collisions at an energy of 1.93 AGeV and zero impact parameter. It is seen that the maximum baryon density reached in the central region is around three times normal nuclear density, while the maximum delta and pion densities are about 1/6 of the maximum nucleon density. The abundance of pions and deltas is given in the lower window of Fig. 8, which shows that the maximum number of delta is around 18. Since the number of pions reaches around 30 at freeze out, the pion/nucleon ratio is thus about 0.25, which is in agreement with the experimental data [62] as well as other transport model results [63].

Our results for proton and  $\pi^-$  rapidity distributions are compared with the experimental data from the FOPI collaboration [24] in Fig. 9, where  $\bar{y} = y/y_{\text{projectile}}$  is the normalized center-of-mass rapidity. The theoretical results are obtained for the impact parameter range  $b \leq 2$  fm in order to compare appropriately with the data which have a centrality selection of 100 mb. Also, only protons that have a local density less than  $0.02 \text{ fm}^{-3}$  at freeze out are included. Otherwise, they are considered as bounded in the deuteron and other light fragments. The agreement between theoretical results and data, especially in mid-rapidity region, is quite good, so we feel that our transport model describes properly the dynamics

of nucleons, deltas, and pions. The proton rapidity distribution shows a peak at  $\bar{y} = 0$ , thus indicating that considerable amount of stopping is achieved in the collisions.

In Fig. 10, the nucleon and pion transverse mass distributions at mid-rapidity region ( $-0.2 < y < 0.2$ ) are shown. We find that the inverse slope parameter for nucleons is about 180 MeV, while that of pions is about 120 MeV. The difference is due to radial flow, which has a larger effect on nucleons than pions.

### C. The kaon yield and distribution

The abundance of kaons and antikaons is shown in Fig. 11. Without kaon medium effects the  $K^+$  number reaches about 0.18, while that of  $K^-$  reaches about  $1.4 \times 10^{-3}$ . Including kaon medium effects, the kaon yield is reduced by about 20% to about 0.15, while the  $K^-$  yield increases by about a factor of 3 to about  $4 \times 10^{-3}$ . In our model,  $K^+$  feels a weak repulsive potential in nuclear matter, which increases its production threshold and thus reduces the yield slightly. On the other hand,  $K^-$  has a strong attractive potential, so its production threshold is reduced and a much larger yield is obtained.

The kaon and antikaon rapidity distributions for central Ni+Ni collisions are shown in Fig. 12 for both cases with and without kaon medium effects. As in the case of pions and nucleons, the rapidity distributions peak at  $y = 0$ . In Fig. 13, the kaon and antikaon transverse mass distributions in mid-rapidity region ( $-0.2 < y < 0.2$ ) are shown. For kaon, the inverse slope parameter is found to be about 100 MeV without kaon medium effects, and increases to about 120 MeV after kaon medium effects are included. The kaon momentum thus increases as a result of propagation in the repulsive mean-field potential. For antikaon, an inverse slope parameter of about 110 MeV is found in the case without kaon medium effects. This is somewhat larger than that of the kaon transverse mass spectra, mainly due to the absorption of low-momentum antikaons by nucleons because of a larger absorption cross section [57]. Including kaon medium effects, the inverse slope parameter decreases to about 100 MeV. The propagation in the mean-field potential thus reduces the antikaon

momentum as a result of the attractive potential. Therefore, from the ratio of kaon and antikaon transverse mass spectra it is possible to learn about the kaon medium effects as pointed out in Ref. [64].

## IV. PHI MESON PRODUCTION FROM HEAVY ION COLLISIONS

### A. Transport model for the phi meson

Phi mesons are also treated in our model by the perturbative test particle method [49]. Whenever a pion-baryon or a baryon-baryon collision is above the threshold for phi meson production, a phi meson is produced and is assigned a probability factor that is given by the phi meson production cross section to the total pion-baryon or baryon-baryon cross section. The motion of the phi meson, including its collisions with other nucleons, is then followed. As in the case of kaon, effects of these collisions are included for phi mesons but not nucleons. The numerical simulation of heavy ion collisions is stopped when the number of collisions is small. The number of phi mesons at this time is taken to be the yield accessible to measurement by identifying  $K\bar{K}$  pairs. As shown in Refs. [50,57],  $KN$  and  $\bar{K}N$  scattering are significant before freeze out, so the  $K\bar{K}$  pair coming from the phi meson decay inside the fireball lose their correlation before they get out and cannot be identified as a phi meson from the  $K\bar{K}$  invariant mass spectrum.

In  $\pi N$  or  $\pi\Delta$  channels phi meson is produced in a two-body final state, so the magnitude of its momentum is fixed by kinematics. The polar angle of the phi meson momentum depends on the differential cross section and is thus determined by a probability function given by the ratio of the differential cross section to the total cross section. For the azimuthal angle of the momentum, it has a uniform distribution between zero and  $2\pi$ .

The baryon-baryon channels are more complex as the phi meson is produced in a three-body final state. In this case, the final momentum of the phi meson follows a multivariable probability function given by the ratio of the differential cross section to the total cross

section. To simplify the numerical procedure, we assume that the phi meson is produced isotropically in the baryon-baryon center of mass frame as discussed in Section II B. This assumption is often used in transport model study when no data exist for the differential cross section. The magnitude of phi meson momentum is then determined by the momentum spectrum such as that shown in Fig. 6

When including medium effects, we only change the available phase space due to the modification of hadron masses. Modifications on coupling constants, cut-off parameters, and the functional form of cross sections are neglected in this study. In the case of a reaction  $A + B \rightarrow C + D$ , the functional form of the cross section as a function of  $E(= \sqrt{s^*} - \sqrt{s_0^*})$  is assumed to be the same as in free space, where the modified center of mass  $\sqrt{s^*}$  energy is given by  $\sqrt{s^*} = \sqrt{p_A^{*2} + m_A^{*2}} + \sqrt{p_B^{*2} + m_B^{*2}}$ , while the modified production threshold is  $\sqrt{s_0^*} = m_C^* + m_D^*$ , with  $p^*$  and  $m^*$  being the momentum and mass of a particle in nuclear medium.

In our study medium modifications of pion properties are neglected, while those on nucleons are always included. For the treatment of kaon, antikaon and phi meson production, we will consider three scenarios. In the first scenario, we neglect medium effects on both kaons and phi mesons. It is already known from previous studies of antikaon production [57,60] that the neglect of kaon medium effects underestimates the antikaon yield. In the second scenario, we include medium effects on kaons but neglect those on phi mesons. The kaon medium effects are obtained from the chiral perturbation calculation as discussed earlier. Inclusion of kaon medium effects improves the agreement of the antikaon yield with the experimental data as discussed in Section III C. Since a phi meson decays mainly into a kaon-antikaon pair, medium modifications of kaon properties affect the final phi meson yield determined from the reconstruction of  $K^+K^-$  pairs. In the last scenario, we include both kaon and phi meson medium effects. For the in-medium phi meson mass we use the results from QCD sum rule calculations by Hatsuda and Lee [4],

$$\frac{m_\phi^*}{m_\phi} \approx 1.0 - 0.0225 \frac{\rho}{\rho_0}, \quad (11)$$

which is obtained by taking the nucleon strangeness content to be about 0.15.

## B. The phi meson yield

The results for phi meson yield in central Ni+Ni collisions at 1.93 AGeV are shown in Fig. 14. Phi mesons are mostly produced during the first 10 fm/c, so the yield increases with time. Afterwards, phi meson decay and reabsorption become more important, and the phi meson yield is seen to decrease with time. We find that at  $t \approx 22$  fm/c two-body scattering becomes rather scarce, so we take this as the freeze-out time and determine the final phi meson yield by the number of phi mesons which have not decayed.

In the scenario that both kaon and phi meson medium effects are neglected, the phi meson yield has a value of  $3.3 \times 10^{-4}$ , while that of  $K^-$  is about  $1.4 \times 10^{-3}$ . The  $\phi/K^-$  ratio in central collision is thus about 25% and is about a factor of 2 too large compared with preliminary FOPI data. However, as pointed out earlier [57,60], the  $K^-$  yield without medium effects is inconsistent with experimental results. In order to explain the observed  $K^-$  yield, kaon medium effects are needed, and this will increase  $K^-$  yield by about a factor of 3. The  $\phi/K^-$  ratio would then be about 8% and is in reasonable agreement with the FOPI data.

On the other hand, the inclusion of kaon medium effects inevitably affects the phi decay width. With a lower in-medium  $K\bar{K}$  threshold, the phi meson decay width increases significantly [14], so the probability for a phi meson to decay inside the dense matter is enhanced. Because of strong final-state interactions of kaons and antikaons, these phi mesons cannot be identified from  $K^+K^-$  reconstruction. Including this effect we find that the final phi meson yield is reduced by about a factor of 2 to about  $1.6 \times 10^{-4}$ . The  $\phi/K^-$  ratio is now about 4% and is about a factor of three too small compared to the FOPI data.

Including also the dropping of phi meson mass in dense matter leads to an increase of phi meson yield, as a result of lower production threshold. For example, around  $2\rho_0$  where most phi mesons are produced, the reduction in the production threshold is about 45



MeV. The final phi meson yield after including both kaon and phi meson medium effects is about  $3 \times 10^{-4}$ , so the  $\phi/K^-$  ratio is brought back to about 8%, and is again in reasonable agreement with preliminary data from the FOPI collaboration.

In Figs. 15, 16, and 17, the phi meson yield from different production channels is shown for the three scenarios mentioned above. In all three cases the  $\pi N$  channel is the dominant one, contributing about 60% of the total phi meson yield. The importance of the  $\pi N$  channel is due to its large cross section near the threshold, although pions have a lower abundance than that of nucleons and the production threshold for this process is also the highest. The baryon-baryon channels add up to about 15-20% of the total phi meson yield, with  $N\Delta$  contributing the most. If phi meson production cross sections in  $N\Delta$  and  $\Delta\Delta$  collisions are assumed to be the same as that in  $NN$  collisions, we find that the final phi meson yield is reduced by about 10%, with the baryon-baryon contribution being only about 5-10% of the total. In the scenario that both kaon and phi meson medium effects are neglected, the  $K\bar{K}$  channel contributes only about 7% of the total phi meson yield. Inclusion of kaon medium effects increases it slightly to about 12% of total phi meson yield.

The impact parameter dependence of phi meson yield in Ni+Ni collisions at 1.93 AGeV is shown in Fig. 18. From this, the minimum-biased phi meson production cross section can be estimated. It is about 0.15 mb when both kaon and phi medium effects are neglected. This reduces to about 0.05 mb if kaon medium effects are included but those on phi mesons are neglected. Including both kaon and phi meson medium effects increases the production cross section to about 0.13 mb.

Both phi meson decay and absorption have significant effects on its final yield. Without kaon medium effects, about 20% of produced phi mesons are absorbed in  $\phi N$  scattering, and about another 20% decay before freeze out. Including kaon medium effects, absorption by nucleons still removes about 20% of produced phi mesons, but phi meson decay is significantly enhanced, leading to more than 50% reduction of the phi meson yield.

### C. The phi meson rapidity distribution and transverse mass spectrum

The rapidity distribution and transverse mass spectrum of phi mesons at freeze out are shown in Fig. 19 and Fig. 20, respectively. The phi meson rapidity distribution is seen to peak at  $y = 0$  as those of nucleons, pions, and kaons. Their transverse mass distribution has a typical exponential form with an inverse slope parameter of about 110 MeV for all three scenarios considered.

The results shown in the above include  $\phi N$  scattering with a cross section of 0.56 mb. To see more clearly the effects due to scattering we show in Fig. 21 the phi meson transverse mass spectra with and without  $\phi N$  elastic scattering in the scenario of no medium effects on kaons and phi mesons. To facilitate the comparison, different results are normalized to have the same value at  $m_t - m_\phi = 25$  MeV. We find that the inverse slope parameter for phi mesons in the mid-rapidity region, obtained by fitting the spectrum up to 0.4 GeV, changes only slightly when rescattering is included. As the extraction of  $\phi N$  elastic cross section from the experimental data is model-dependent, its value may not be well determined. To see the effects due to a different cross section, we have also repeated the calculation using a  $\phi N$  elastic cross section of 8.3 mb, which is the total  $\phi N$  cross section estimated from the phi meson photoproduction data [65] and serves as an upper bound on the elastic cross section. The inverse slope parameter in this calculation is found to be about 130 MeV. The increase of the slope parameter due to scattering can be understood as follows. At SIS energies most produced phi mesons have low momenta, so scattering with nucleons increases their momenta and helps them in achieving thermalization with nucleons. Similar effects have been found for kaons in heavy ion collisions at subthreshold energies [50,66].

## V. SUMMARY AND OUTLOOK

We have carried out a transport model study of phi meson production from heavy ion collisions at SIS energies. The production channels included in our study are  $\pi N \rightarrow \phi N$ ,

$\pi\Delta\longrightarrow\phi N$ ,  $NN\longrightarrow NN\phi$ ,  $N\Delta\longrightarrow NN\phi$ ,  $\Delta\Delta\longrightarrow NN\phi$ , and  $K\bar{K}\longrightarrow\phi$ . The cross sections for the first five reactions are obtained from the one-boson-exchange model, while that for the last one is taken to be of Breit-Wigner form through the phi meson resonance. More than half of the phi mesons are found to be produced from  $\pi N$  collisions.

The predicted  $\phi/K^-$  ratio depends on whether medium effects are included for kaons and phi mesons. Neglecting both kaon and phi medium effects, the ratio is about 25%, which is about a factor of two larger than that from the FOPI data. However, the  $K^-$  yield in this case is about a factor of 3 below the measured value. To account for the observed  $K^-$  yield requires the inclusion of medium effects on kaons, such as that predicted by the chiral perturbation theory, so that the antikaon production threshold is reduced. The  $\phi/K^-$  ratio turns out to be about a factor of 2-3 smaller than the experimental results. Including also dropping phi meson mass in nuclear medium as predicted by the QCD sum rules increases the phi meson yield. The final  $\phi/K^-$  ratio becomes about 8% and agrees reasonably with the preliminary FOPI data.

It will be of interest to also measure phi mesons through their dilepton decay channel, which will be carried out in the near future by the HADES collaboration [67] at GSI. Since both the  $K\bar{K}$  and the dilepton channels are subject to same uncertainties in the production mechanism, the ratio of the phi meson yield measured from the  $K\bar{K}$  channel to that measured from the dilepton channel is expected to be less sensitive to such uncertainties. In addition, the dilepton channel can also reveal directly the properties of vector mesons in nuclear medium, especially the change in their masses [63,68,69]. For phi mesons, this is not possible via the  $K\bar{K}$  channel since the correlation of a  $K\bar{K}$  pair is lost due to  $KN$  scattering in the nuclear medium. Furthermore, the shape of the phi meson peak in the dilepton spectrum can also indirectly give information on the kaon medium effects [70]. For this purpose, a careful study of the background is needed to determine whether the phi meson peak will still be observable. Previous study [63] shows that the background due to nucleon and pion bremsstrahlung as well as the eta Dalitz decay is small near the phi meson peak. The major background is thus expected to come from decays of rho and omega

mesons. A careful study of the production of vector mesons in heavy ion collisions is needed in order to learn the phi meson properties from the dilepton decay channel. Such a study is in progress.

### **Acknowledgement**

We acknowledge useful discussions with R. Machleidt. We also thanks J. A. M. Vermaseren for his program FORM (version 1.1) and P. Lepage for his subroutine VEGAS, which we have used extensively in evaluating the elementary cross sections for phi meson production. This work was supported in part by the National Science Foundation under Grant No. PHY-9509266. GQL was also supported in part by the Department of Energy under Contract No. DE-FG02-88Er40388.

## REFERENCES

- [1] A. Shor, Phys. Rev. Lett., 54 (1985) 1122.
- [2] S. Okubo, Phys. Lett. 5 (1963) 165; J. Iizuka, Prog. Theo. Phys. Suppl. 37-38 (1966) 21.
- [3] G. E. Brown and M. Rho, Phys. Rev. Lett. **66** (1991) 2720.
- [4] T. Hatsuda and S. H. Lee, Phys. Rev. C 46 (1992) R34; T. Hatsuda, Nucl. Phys. A 544 (1992) 27c.
- [5] M. Asakawa and C.M. Ko, Nucl. Phys. A 572 (1994) 732.
- [6] G. E. Brown and M. Rho, Phys. Rep. 269 (1996) 333.
- [7] C. M. Ko and G. Q. Li, J. of Phys. G 22 (1996) 1673.
- [8] C. M. Ko, V. Koch, and G. Q. Li, Ann. Rev. Nucl. Part. Sci., in press.
- [9] C. M. Ko, P. Lévai, X. J. Qiu, and C. T. Li, Phys. Rev. C 45 (1992) 1400.
- [10] H. Kuwaraba and T. Hatsuda, Prog. Theor. Phys. 94 (1995) 1163c.
- [11] C. S. Song, Phys. Lett. B 388 (1996) 1410.
- [12] C. M. Ko and B. H. Sa, Phys. Lett. B 258 (1991) 6.
- [13] F. Karsch, K. Redlich, and L. Turko, Z. Phys. C 60 (1993) 519.
- [14] G. Q. Li and C. M. Ko, Nucl. Phys. A 582 (1995) 731.
- [15] M. Asakawa and C. M. Ko, Phys. Lett. B 322 (1994) 33; Phys. Rev. C 50 (1994) 3064.
- [16] R. Ferreira, Nucl. Phys. A 544 (1992) 497c.
- [17] M. A. Mazzoni, Nucl. Phys. A 566 (1994) 95c.
- [18] M. Berenguer, H. Sorge, and W. Greiner, Phys. Lett. B 332 (1994) 15.

- [19] P. Koch, U. Heinz, and J. Pisút, Phys. Lett. B 243 (1990) 149.
- [20] B. A. Cole, E802 Collaboration, Nucl. Phys. **A590** (1995) 179c; Y. Akiba *et al*, Phys. Rev. Lett. 76 (1996) 2021.
- [21] P. Braun-Munzinger, J. Stachel, J. P. Wessels, and N. Xu, Phys. Lett. B 344 (1995) 43.
- [22] J. Cleymans, D. Elliott, H. Satz, and R.L. Thews, nucl-th/9603004.
- [23] A. J. Baltz and C. Dover, Phys. Rev. C 53 (1996) 362.
- [24] N. Herrmann for FOPI Collaboration, in: Proc. Quark Matter '96, Nucl. Phys. A 610 (1996) 49c.
- [25] W. Cassing, V. Metag, U. Mosel, and K. Niita, Phys. Rep. 188 (1990) 363.
- [26] U. Mosel, Ann. Rev. Nucl. Part. Sci. 41 (1991) 29.
- [27] W. S. Chung, G. Q. Li, and C. M. Ko, Phys. Lett. B, in press.
- [28] D. B. Kaplan and A. E. Nelson, Phys. Lett. B 175 (1986) 57; A. E. Nelson and D. B. Kaplan, Phys. Lett. B 192 (1987) 193.
- [29] C. H. Lee, G. E. Brown, D. P. Min, and M. Rho, Nucl. Phys. A 585 (1995) 401.
- [30] A. Baldini *et al.*, Total cross sections of high energy particles, (Springer-Verlag, Heidelberg, 1988).
- [31] R. Baldi *et al.*, Phys. Lett. B68 (1977) 38; M. W. Arenton *et al.*, Phys. Rev. D 25 (1970) 2241; V. Blobel *et. al.*, Phys. Lett. B 59 (1975) 88.
- [32] R. Machleidt, Adv. Nucl. Phys. 19 (1989) 189.
- [33] A. A. Sibirtsev, Nucl. Phys. A 604 (1996) 455.
- [34] R. F. Peierls, Phys. Rev. Lett. 6 (1961) 641.
- [35] B. Holzenkamp, K. Holinde, and J. Speth, Nucl. Phys. A 500 (1989) 485.

- [36] H. Joos, Phys. Lett. B24 (1967) 103.
- [37] V. Barger and R. J. N. Phillips, Phys. Lett. B58 (1975) 197.
- [38] A. Engel, R. Shaym, U. Mosel, and A. K. Dutt-Mazumder, Nucl. Phys. A 603 (1996) 387.
- [39] W. Peters, U. Mosel, and A. Engel, Z. Phys. A **353** (1995) 333.
- [40] J. M. Laget, Phys. Lett. B 259 (1991) 24.
- [41] G. Q. Li and C. M. Ko, Nucl. Phys. A 594 (1995) 439.
- [42] S. Huber and J. Aichelin, Nucl. Phys. A 573 (1994) 587.
- [43] R. Bertini, Nucl. Phys. A 585 (1995) 265c.
- [44] C. M. Ko, Q. Li, and R. Wang, Phys. Rev. Lett. 59 (1987) 1084; C. M. Ko and Q. Li, Phys. Rev. C 37 (1988) 2270; Q. Li, J. Q. Wu, and C.M. Ko. Phys. Rev. C 39 (1989) 849; C. M. Ko, Nucl. Phys. A 495 (1989) 321c.
- [45] B. D. Serot and J. D. Walecka, Adv. Nucl. Phys. 16 (1986) 1
- [46] G. Q. Li, C. M. Ko, X. S. Fang, and Y. M. Zheng, Phys. Rev. C 49 (1994) 1139.
- [47] G. F. Bertsch and S. Das Gupta, Phys. Rep. 137 (1988) 189.
- [48] P. Danielewicz and G. F. Bertsch, Nucl. Phys. A533 (1991) 712.
- [49] X. S. Fang, C. M. Ko, and Y. M. Zheng, Nucl. Phys. A556 (1993) 499.
- [50] X. S. Fang, C. M. Ko, G. Q. Li, and Y.M. Zheng, Nucl. Phys. A575 (1994) 766.
- [51] G. Q. Li and C. M. Ko, Nucl. Phys. A594 (1995) 460.
- [52] T. Waas, N. Kaiser, and W. Weise, Phys. Lett. B 365 (1996) 12; 379 (1996) 34.
- [53] G. Q. Li and C. M. Ko, Phys. Lett. B 349 (1995) 405.

- [54] J. Randrup and C. M. Ko, Nucl. Phys. A 343 (1980) 579; A 411 (1983) 537.
- [55] J. Cugnon and R. M. Lombard, Nucl. Phys. A 422 (1984) 635.
- [56] K. Tsushima, S.W. Huang, and A. Faessler, Phys. Lett. B 337 (1994) 245; J. Phys. G 21 (1995) 33.
- [57] G. Q. Li, C. M. Ko, and X. S. Fang, Phys. Lett. B 329 (1994) 149.
- [58] W. Zwermann and B. Schürmann, Phys. Lett. B 145 (1984) 315.
- [59] A. Sibirtsev, W. Cassing, and C. M. Ko, Z. Phys. A, in press.
- [60] W. Cassing, E.L. Bratkovskaya, U. Mosel, S. Teis and A. Sibirtsev, Nucl. Phys. A614 (1997) 415.
- [61] C. M. Ko, Phys. Lett. B 120 (1983) 294.
- [62] J. W. Harris *et al.*, Phys. Lett. B 153 (1985) 377; V. Metag, Proc. VI Int. Conf. on Nuclear Reaction Mechanisms, Varenna, June, 1991, ed. E. Gadioli, p. 683.
- [63] Gy. Wolf, W. Cassing, and U. Mosel, Nucl. Phys. A 552 (1993) 549.
- [64] X. S. Fang, C. M. Ko, G. E. Brown, and V. Koch, Phys. Rev. C 47 (1993) 1678.
- [65] H. J. Behrend *et al.*, Phys. Lett. B56 (1975) 408.
- [66] C. David, C. Hartnack, M. Kerveno, J.-Ch. Le Pallec, and J. Aichelin, nucl-th/9611016.
- [67] W. Koenig, in: Proc. Workshop on Dilepton Production in Relativistic Heavy-Ion Collisions, ed. H. Bokemeyer(GSI, Darmstadt, 1994).
- [68] G. Q. Li, C. M. Ko, and G. E. Brown, Phys. Rev. Lett. 75 (1995) 4007; Nucl. Phys. A606 (1996) 568.
- [69] W. Cassing, W. Ehehalt, and C. M. Ko, Phys. Lett. B 363 (1995) 35.
- [70] D. Lissauer and E. Shuryak, Phys. Lett. B 253 (1991) 15; E. Shuryak and V. Thorsson,



Nucl. Phys. A 536 (1992) 739.

# FIGURES

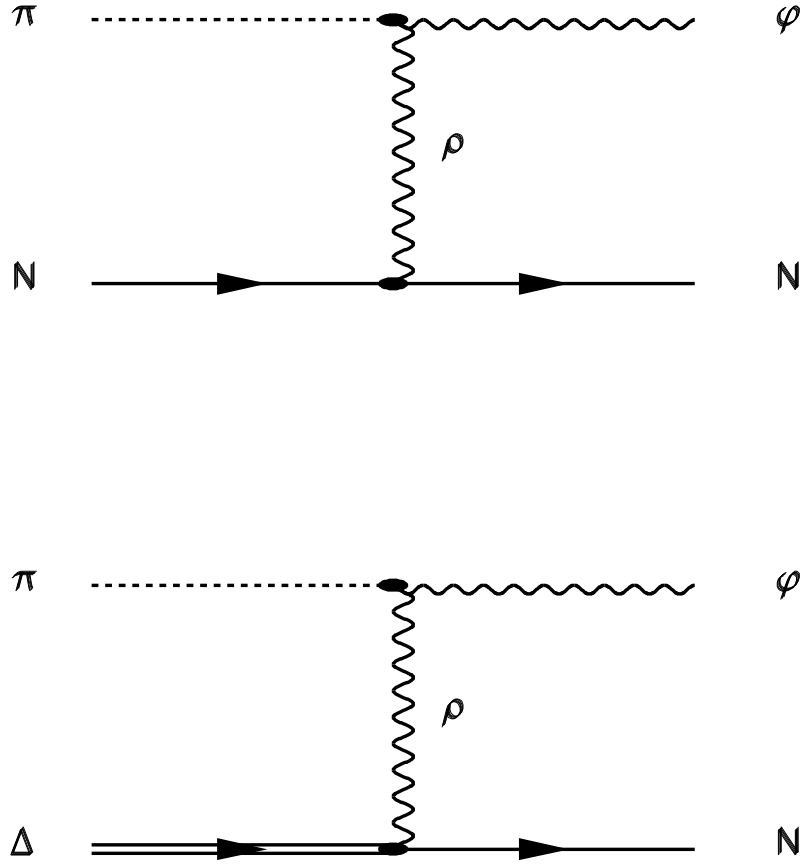


FIG. 1. Feynman diagrams for  $\pi N \rightarrow \phi N$  and  $\pi \Delta \rightarrow \phi N$ .

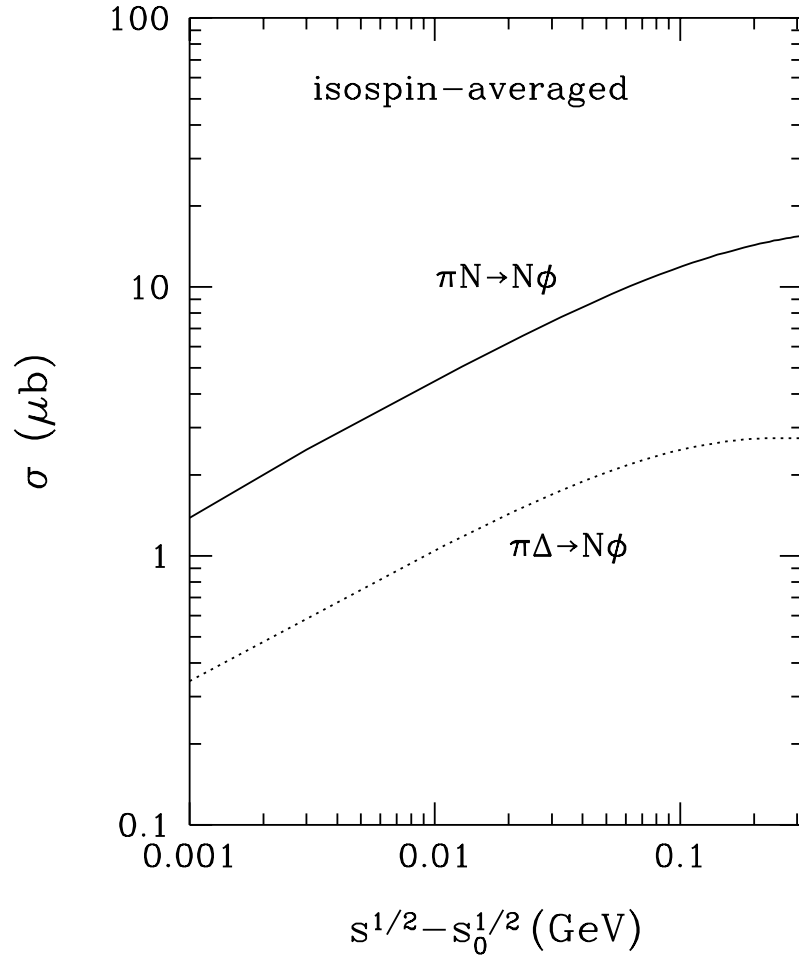


FIG. 2. Isospin-averaged cross sections for  $\pi N \rightarrow \phi N$  (solid curve) and  $\pi\Delta \rightarrow \phi N$  (dotted curve).

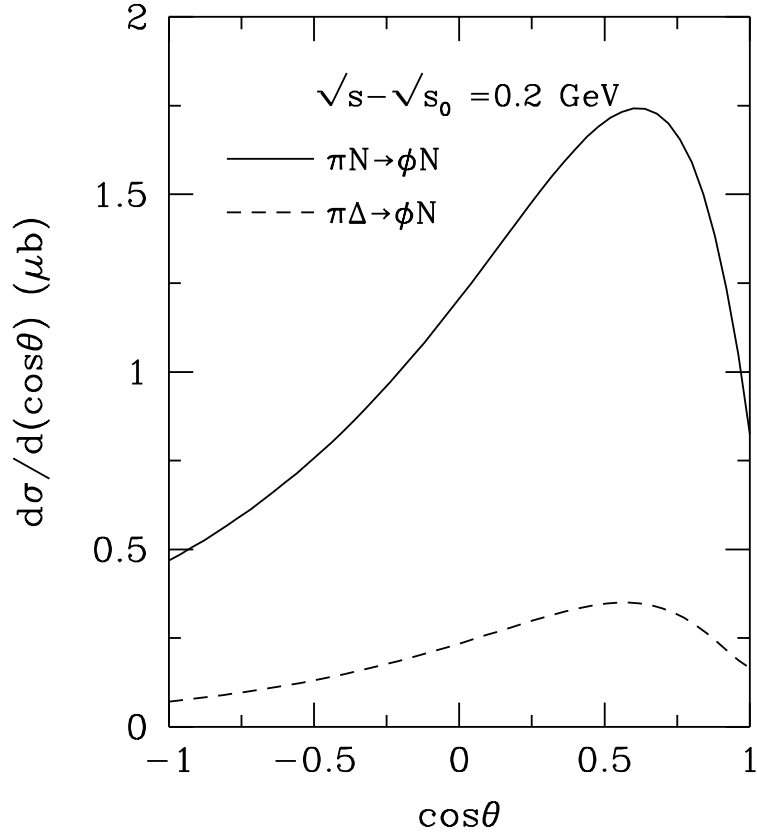


FIG. 3. Differential cross sections for  $\pi N \rightarrow \phi N$  (solid curve) and  $\pi \Delta \rightarrow \phi N$  (dashed curve) at 0.2 GeV above the threshold.

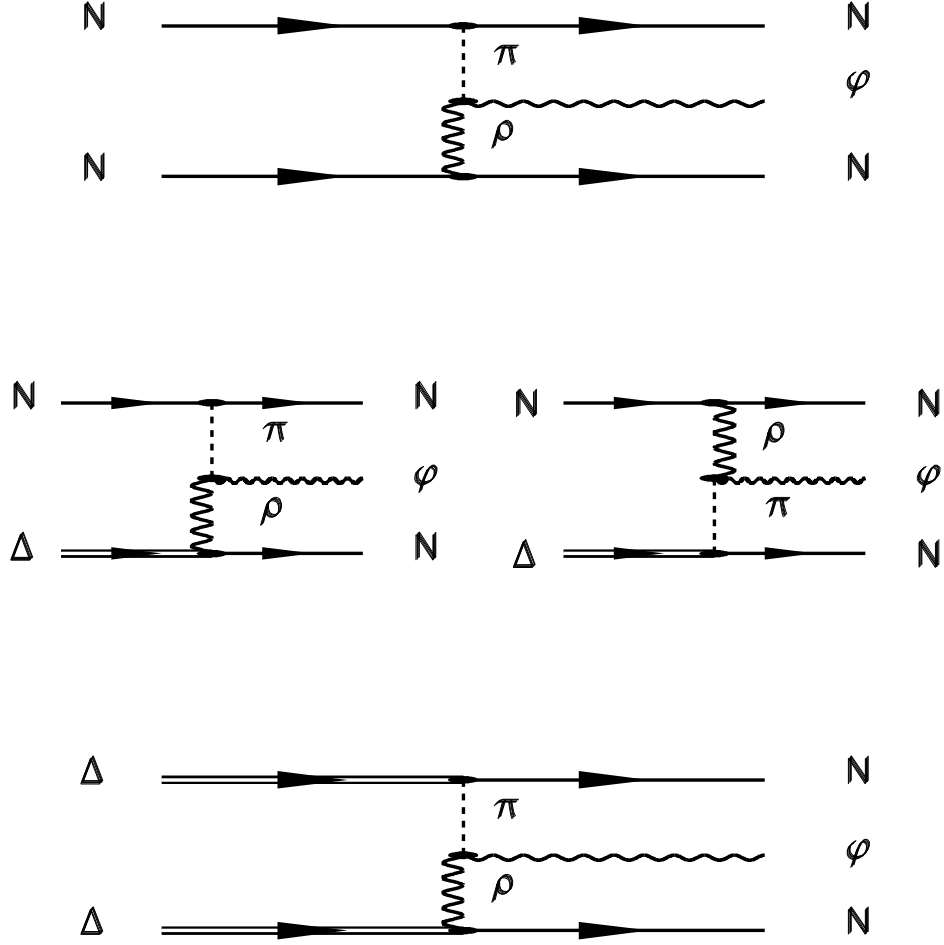


FIG. 4. Feynman diagrams for  $NN \rightarrow NN\phi$ ,  $N\Delta \rightarrow NN\phi$ , and  $\Delta\Delta \rightarrow NN\phi$ .

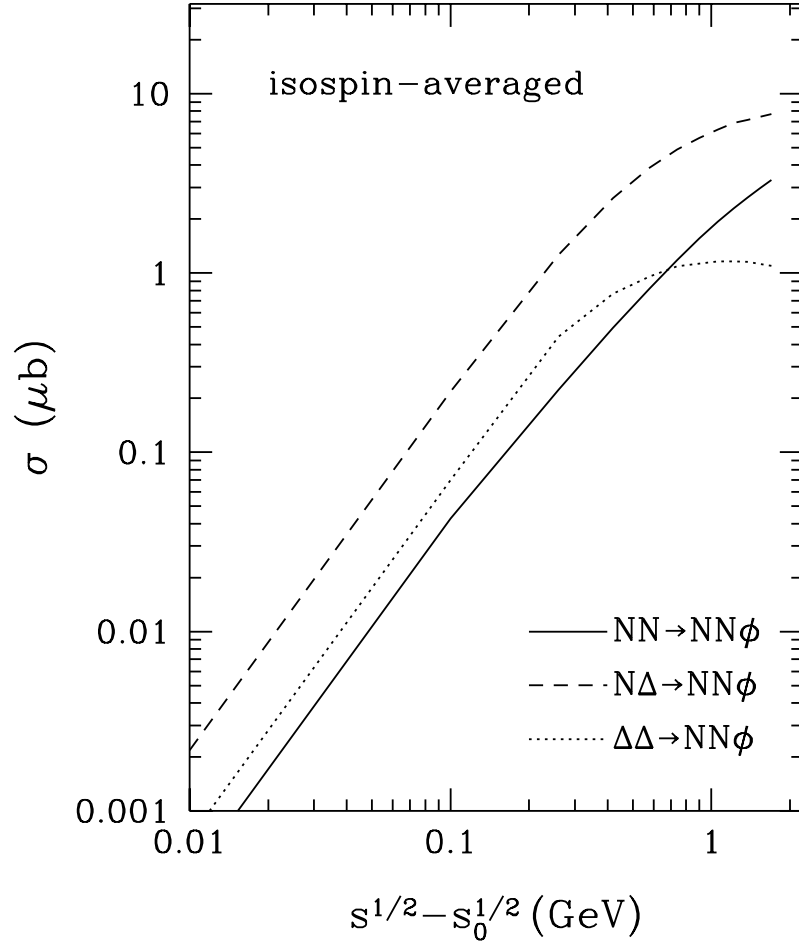


FIG. 5. Isospin-averaged cross sections for  $NN \rightarrow NN\phi$  (solid curve),  $N\Delta \rightarrow NN\phi$  (dashed curve), and  $\Delta\Delta \rightarrow NN\phi$  (dotted curve).

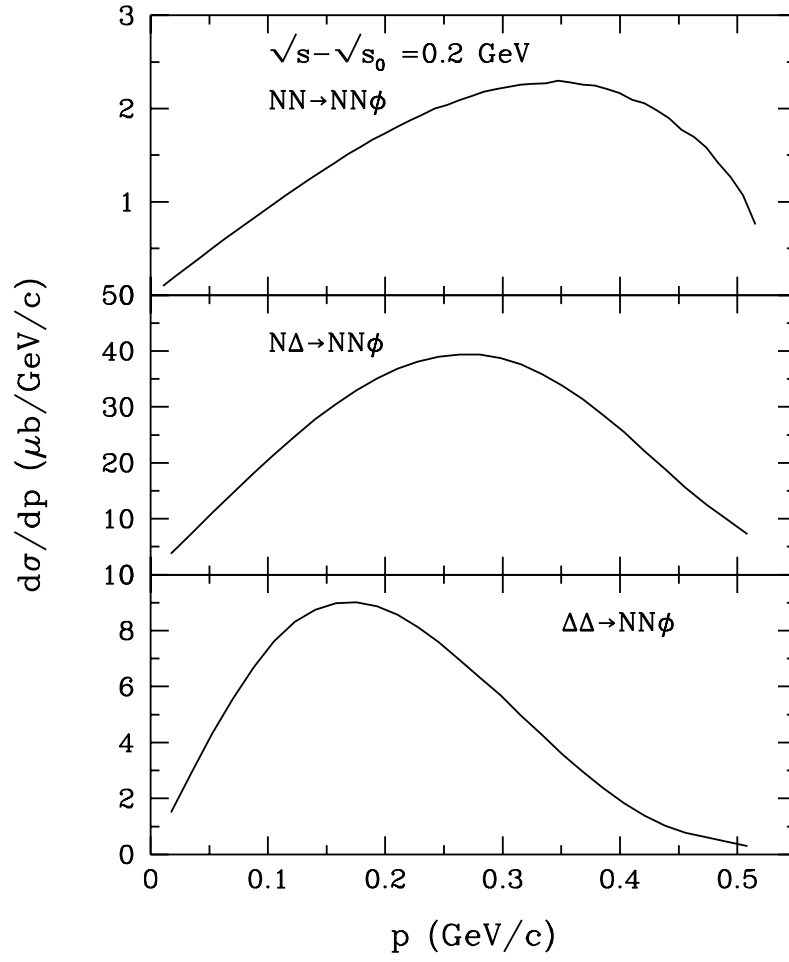


FIG. 6. Phi meson momentum spectrum from the reactions  $NN \rightarrow NN\phi$ ,  $N\Delta \rightarrow NN\phi$ , and  $\Delta\Delta \rightarrow NN\phi$  at 0.2 GeV above the threshold.

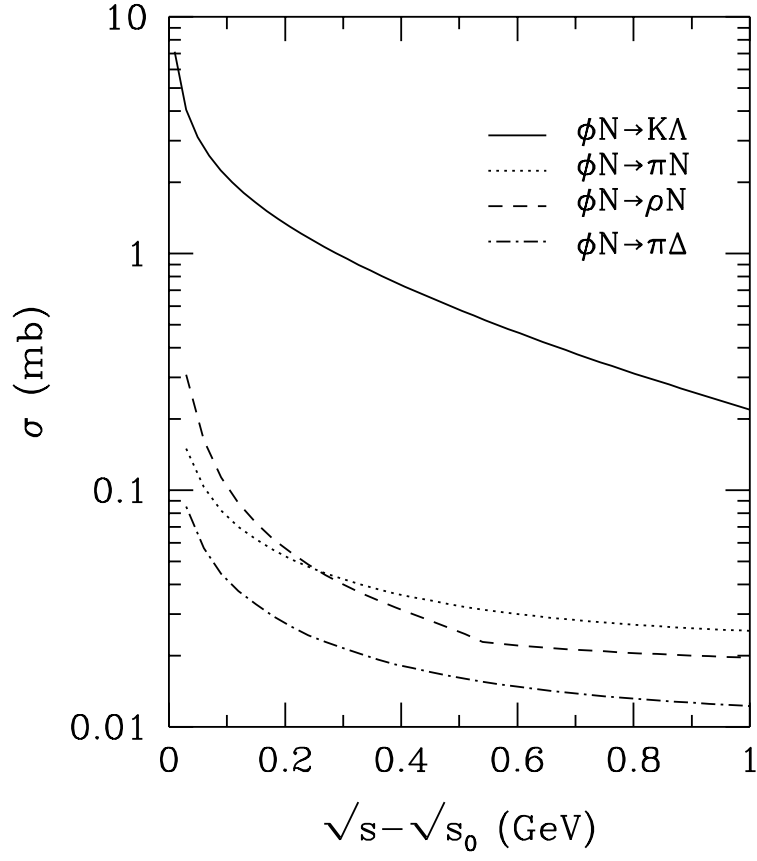


FIG. 7. Cross sections for  $\phi N \rightarrow K\Lambda$  (solid curve),  $\phi N \rightarrow \pi N$  (dotted curve),  $\phi N \rightarrow \rho N$  (dashed curve), and  $\phi N \rightarrow \pi\Delta$  (dash-dotted curve).



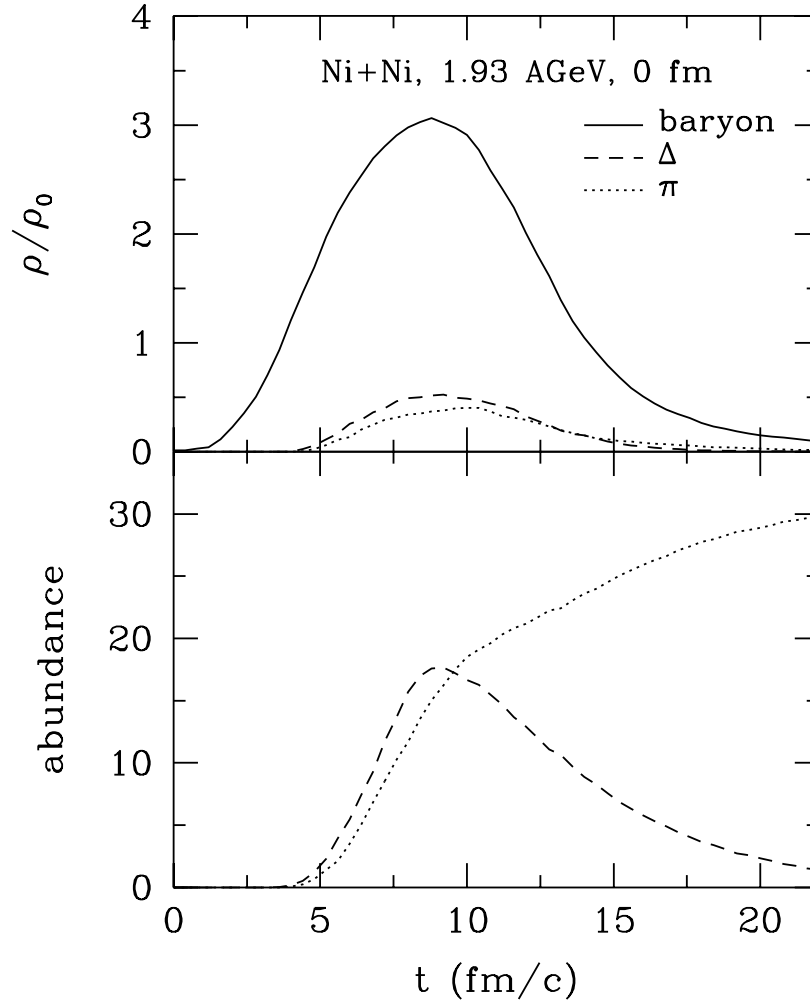


FIG. 8. Upper window: the time evolution of central densities of baryons (solid curve), deltas (dashed curve), and pions (dotted curve) in Ni+Ni collisions at 1.93 AGeV and impact parameter 0 fm. Lower window: the time evolution of the delta (dashed curve) and pion (dotted curve) abundance.

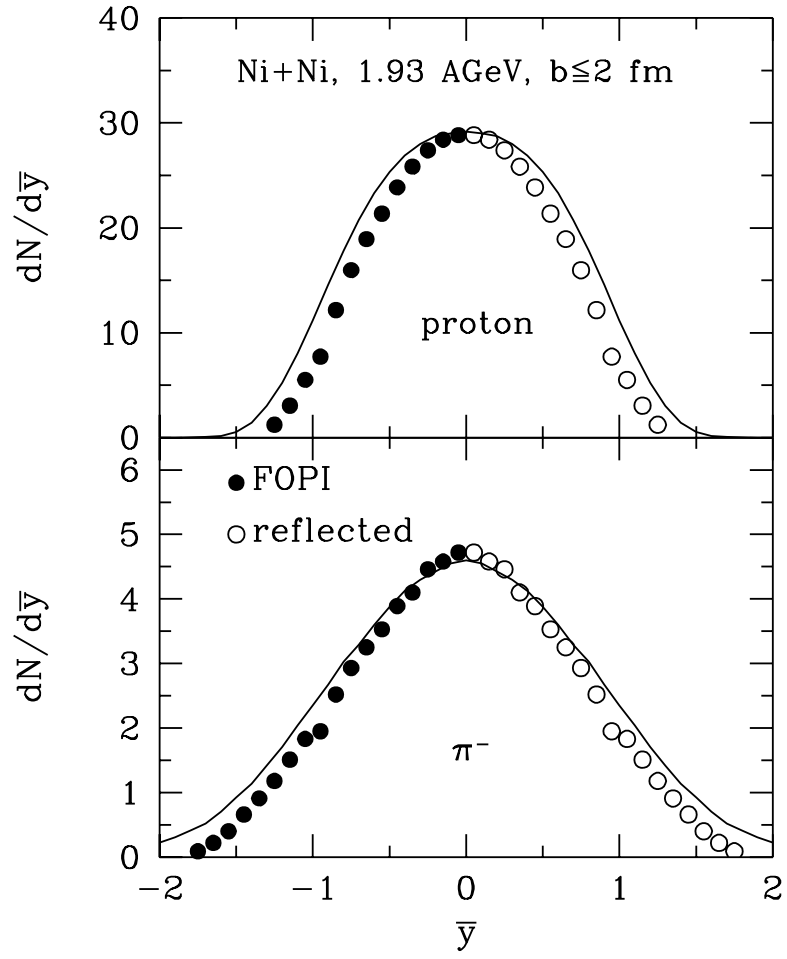


FIG. 9. The rapidity distribution of nucleons and pions in Ni+Ni collisions at 1.93 AGeV and impact parameter  $b \leq 2$  fm.

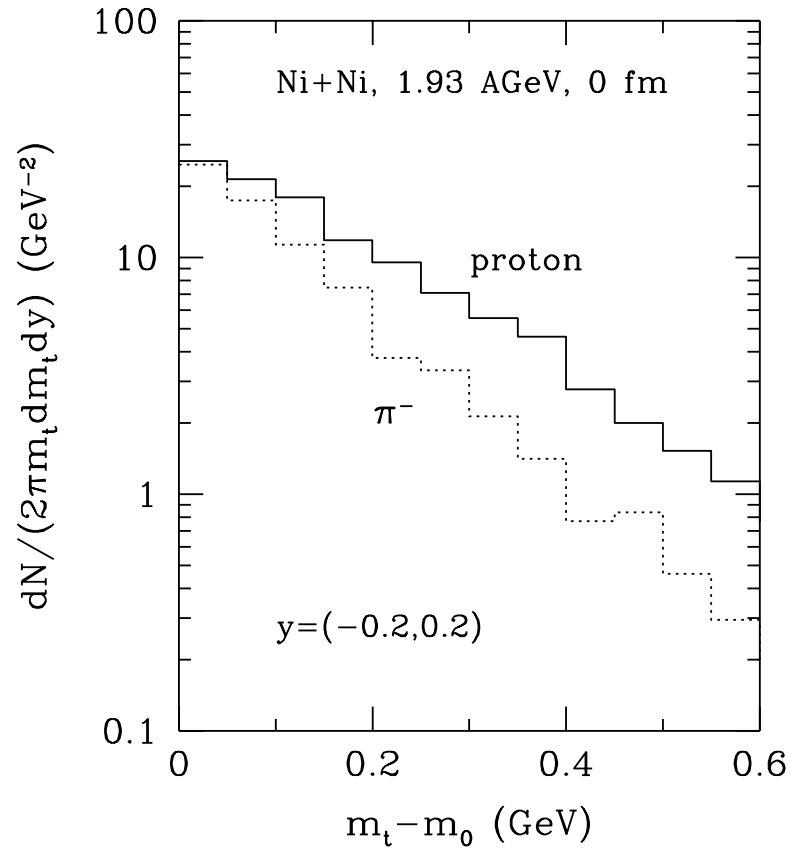


FIG. 10. Same as Fig. 9 for the transverse mass distribution.

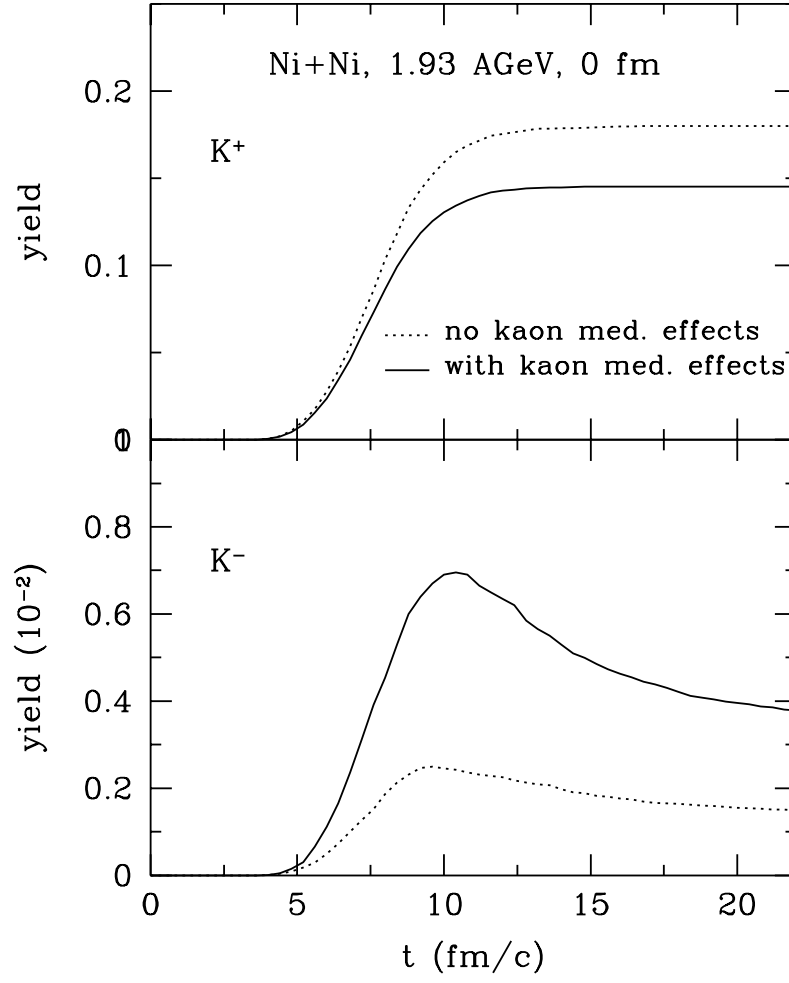


FIG. 11. The abundance of  $K^+$  and  $K^-$  with (solid curve) and without (dotted curve) medium effects in the same reaction as in Fig. 8.

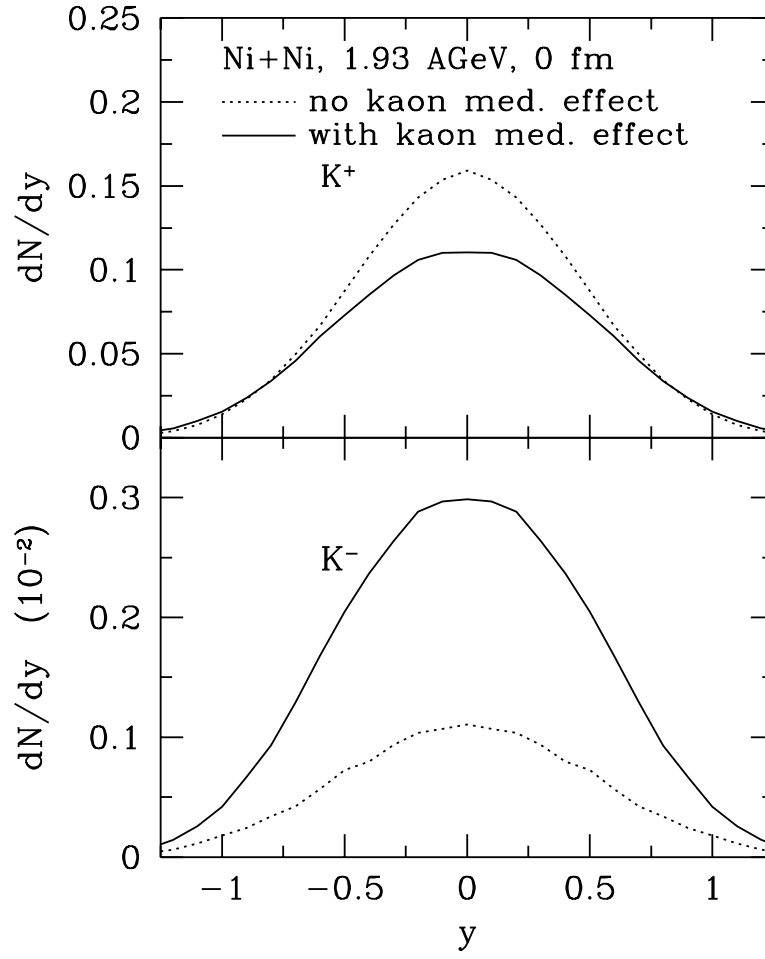


FIG. 12. The rapidity distribution of  $K^+$  and  $K^-$  in central Ni+Ni collisions at 1.93 AGeV with (solid curve) and without kaon (dotted curve) medium effects.

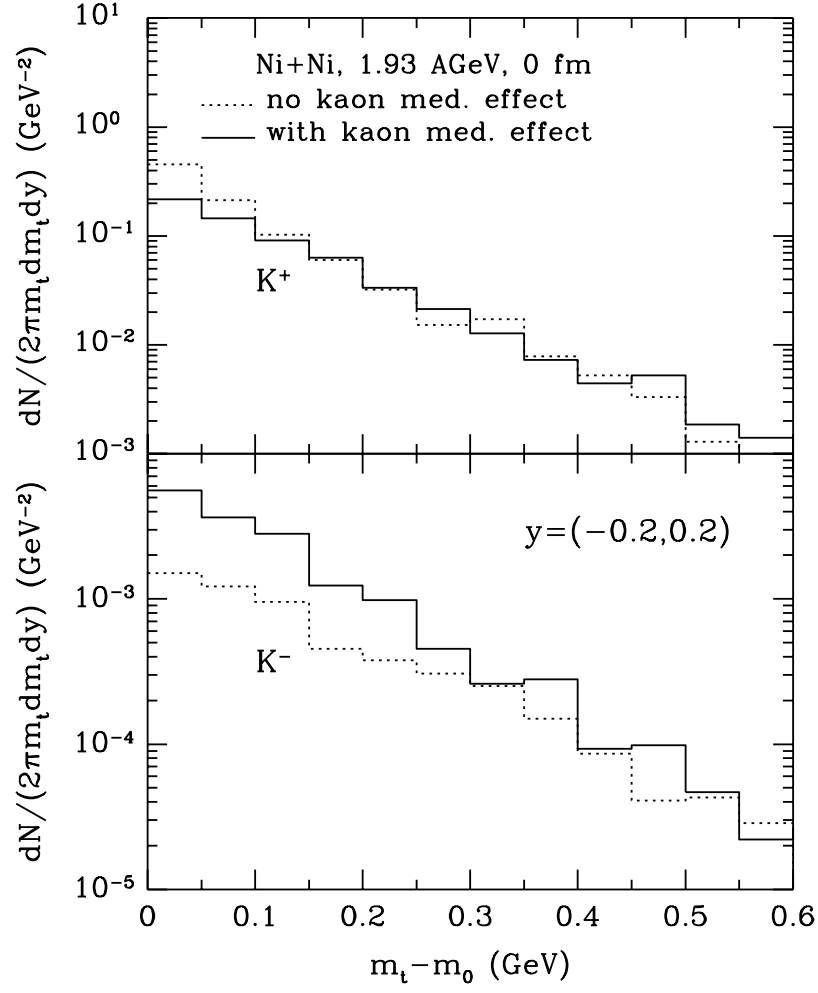


FIG. 13. Same as Fig. 12 for the transverse mass distribution of  $K^+$  and  $K^-$  with (solid curve) and without (dotted curve) medium effects.

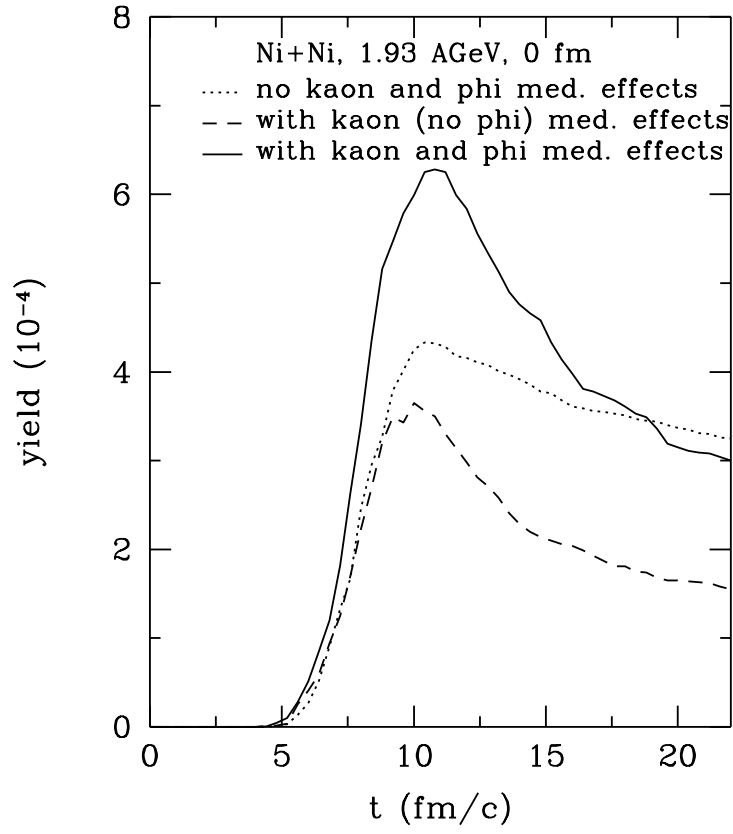


FIG. 14. The phi meson yield in Ni+Ni collision at 1.93 AGeV and impact parameter of 0 fm for three different scenarios.

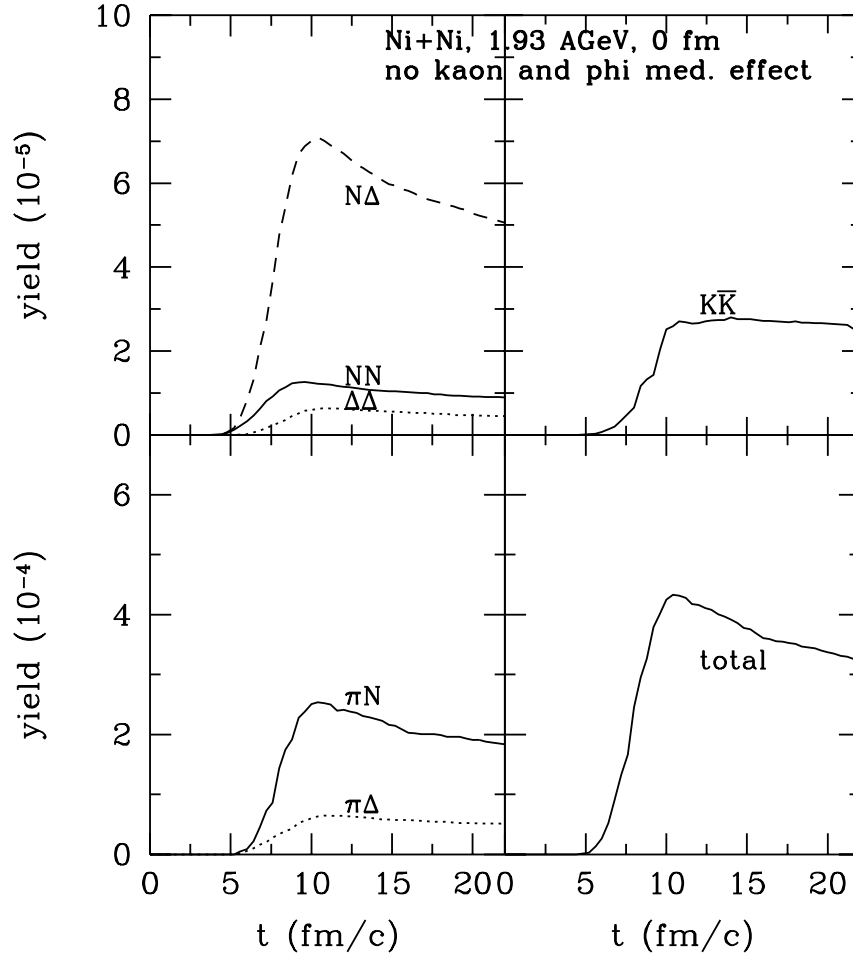


FIG. 15. The time evolution of phi meson yield from different channels in central Ni+Ni collisions at 1.93 AGeV without kaon and phi meson medium effects.



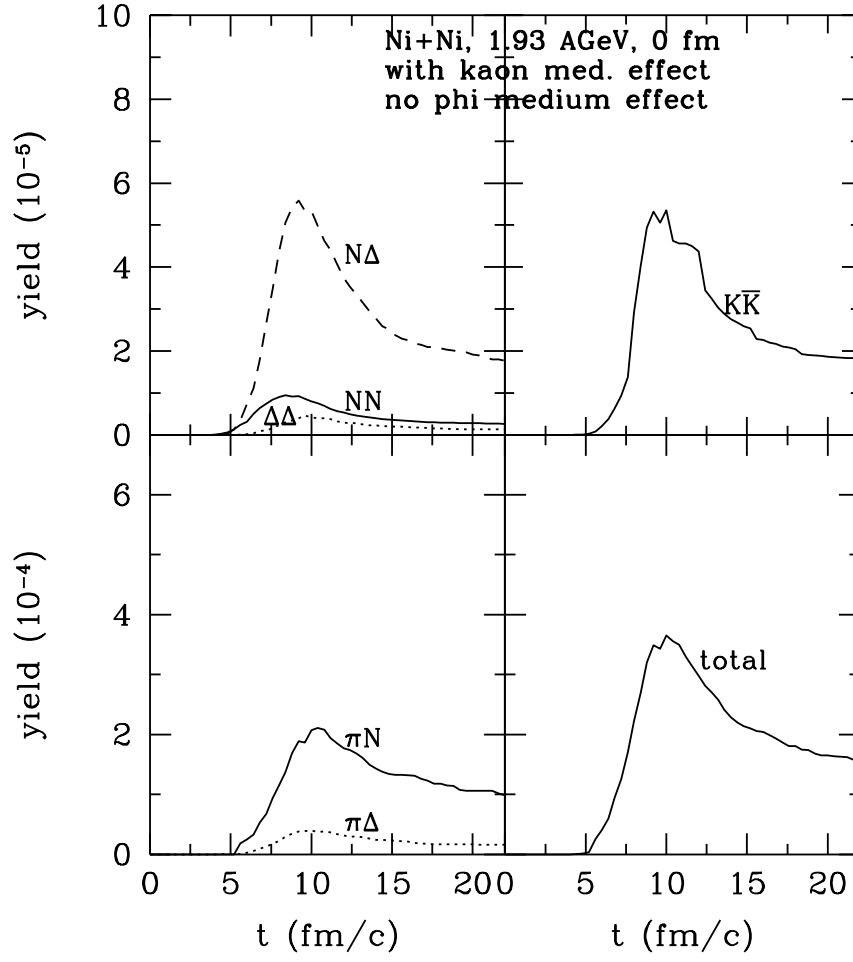


FIG. 16. Same as Fig. 15 with kaon medium effects but no phi meson medium effects.

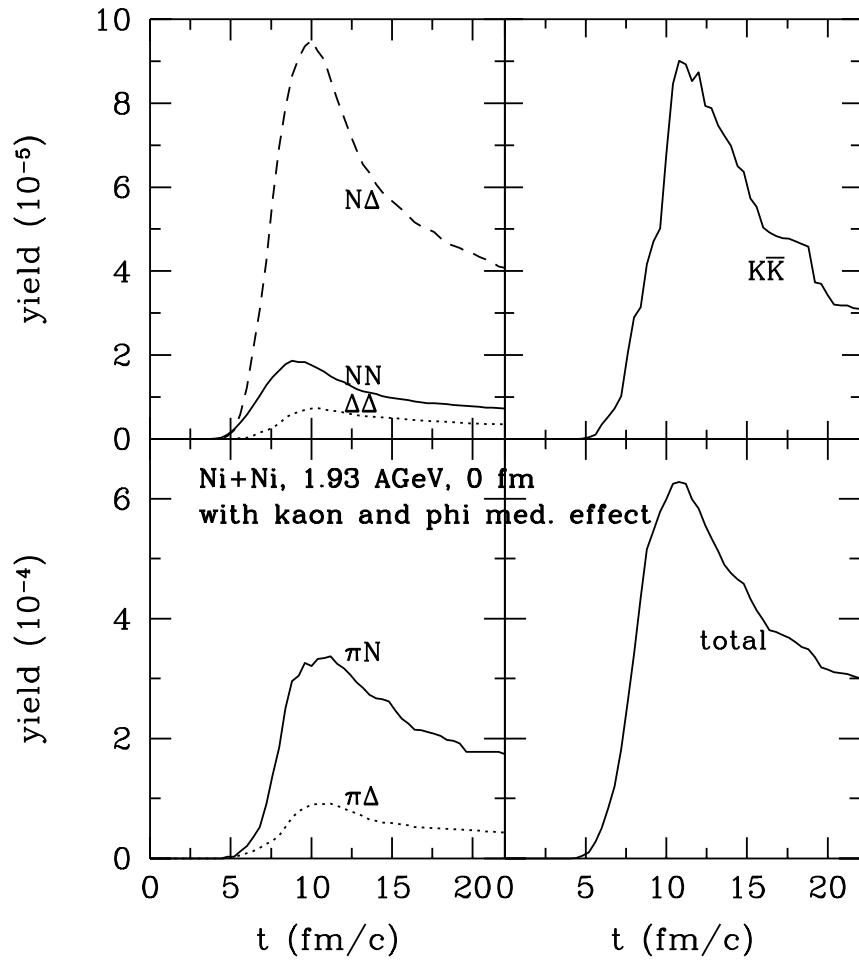


FIG. 17. Same as Fig. 15 with both kaon and phi meson medium effects.

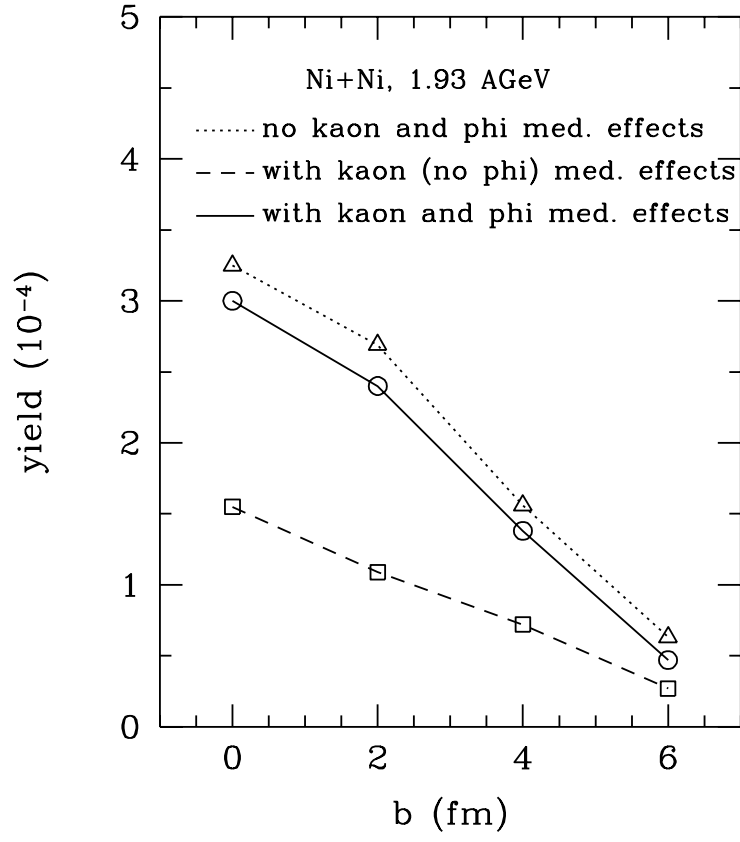


FIG. 18. The phi meson yield in Ni+Ni collision at 1.93 AGeV at different impact parameters for three different scenarios.

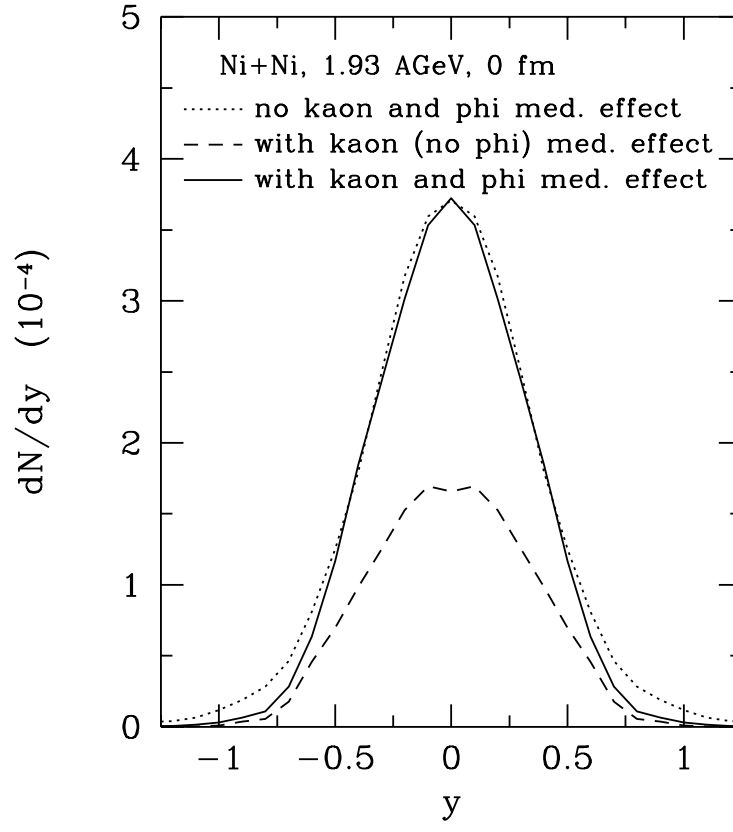


FIG. 19. The rapidity distributions of phi mesons in central Ni+Ni collisions at 1.93 AGeV for three different scenarios.

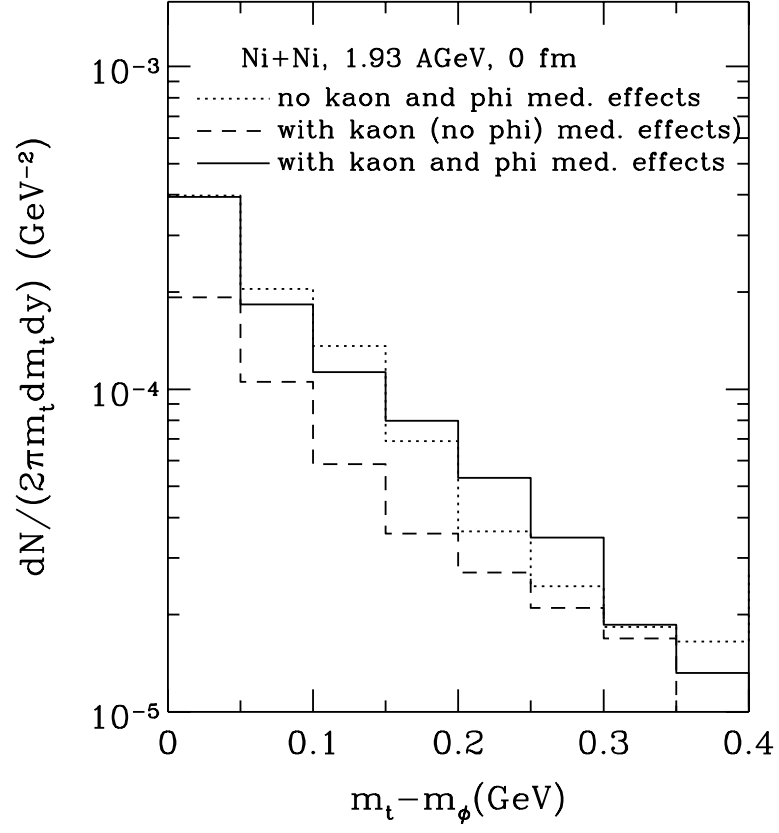


FIG. 20. Same as Fig. 19 for the transverse mass distribution.

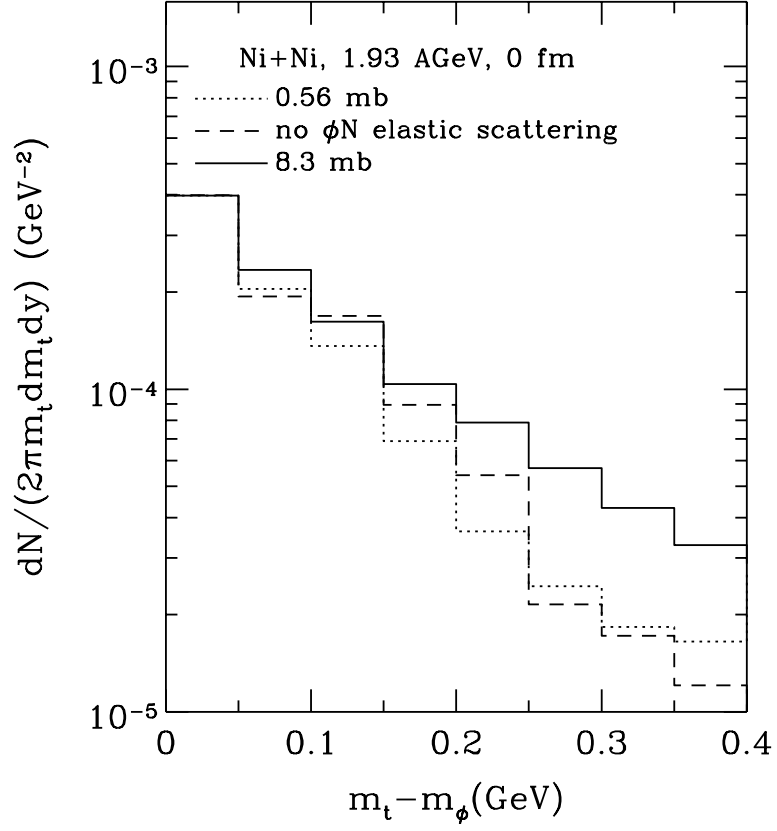


FIG. 21. The transverse mass distribution of phi mesons in central Ni+Ni collisions at 1.93 AGeV with (dotted curve for  $\sigma_{\phi N} = 0.56$  mb and solid curve for  $\sigma_{\phi N} = 8.3$  mb) and without (dashed curve)  $\phi N$  scattering.